J. Heat Treat (1990) 8:127–136

Modeling of the Temperature Field, Transformation Behavior, Hardness and Mechanical Response of Low Alloy Steels during Cooling from the Austenite Region

B. Buchmayr and J.S. Kirkaldy

Abstract. A comprehensive finite element program applicable to all axisymmetric shapes for the prediction of material behavior exposed to various heat treatments has been developed based on a thermodynamic and kinetic algorithm for predicting the hardenability of low alloy steels combined with the calculation of stress and distortion evolution. During the temperature field and stress calculations the microstructural contributions, like latent heat formation, influence on thermophysical properties, microstructural dependence of σ/ε curve, transformation strain, and transformation plasticity are taken into account, which give more insight and more accurate predictions of the material response. Thus microstructural optimizations with respect to hardenability, hardness, residual stresses and distortion are made possible.

Introduction

Heat treatment of low alloy steels is an economical way to produce components with reliable service properties. Both the chemical composition and the kind of heat treatment contribute to the determination of the material properties. Typical examples are induction hardening of gears, controlled heat treatment of rotor forgings, controlled quenching of turbine casings to achieve optimum creep properties, and residual stress reduction in rails.

The objectives of controlling the heat treatment can be classified according to

- reduction of residual stresses
- reduction of distortion
- avoidance of crack initiation
- achievement of sufficient hardenability
- microstructural control to meet improved properties, such as creep strength, wear resistance and toughness
- achievement of a specific hardness distribution

To achieve these particular aims the proper coupling of the calculation parts pertaining to temperature, microstructure, and stress must be effected.

In the past, a number of conferences have been held with special emphasis on the modeling of quenching in order to predict the microstructure and the residual stresses [1–4]. These have provided a better understanding of the underlying processes with which to model the transformation and thermomechanical behavior of low alloy steels during the quenching process.

General System Concept

To describe the microstructural and mechanical phenomena in a correct manner, several interactions or coupling effects have to be considered. Accordingly, a system configuration was chosen as illustrated in

B. Buchmayr is with the Institute for Materials Science and Welding Technology, University of Technology, Graz, Austria. J.S. Kirkaldy is Emeritus Professor with the Institute for Materials Research, McMaster University, Hamilton, Ontario, L8S 4M1.

Figure 1 that deals with the most important coupling effects. The less important coupling phenomena, indicated in brackets, are not included in the current program. It can, for example, be shown that the influence of the deformation heat in a hardening configuration can be ignored because the maximum strain rates which occur at the quenched end are in the order of a few percent per second, which is too low to produce significant temperature changes. This partially coupled configuration allows a stepped routine which first predicts the temperature and simultaneous microstructural evolution and in a second step predicts the mechanical stress/strain response.

The main parts of the software are:

- thermodynamics based prediction of the multicomponent phase diagram corresponding to the chemical steel composition
- analytical prediction of the isothermal transformation diagram
- automatic mesh generation program for the finite element (FE) analysis
- FE calculation of the transient temperature field taking into account microstructural effects such as latent heat
- prediction of the microstructural evolution during quenching incorporating the possibility for intermediate isothermal heat treatments like the austempering process
- FE calculation of the stress/strain response after temperature and microstructure prediction, taking into account dilatation, transformation plasticity, and creep
- prediction of the hardness distribution as a function of microstructure and cooling conditions
- several postprocessing routines for graphical presentation of the results (contouring, hidden line plotting, etc.)

To validate the software the Jominy end-quench bar was examined because for this specimen much reliable experimental data exist for comparison. The program, however, is designed to accommodate any two-dimensional or axisymmetric geometry.

Prediction of the Transformation Behavior

The hardenability concepts developed by Kirkaldy and coworkers [5–8] calibrated to the USS Atlas of Transformation Diagrams were used as a prepro-

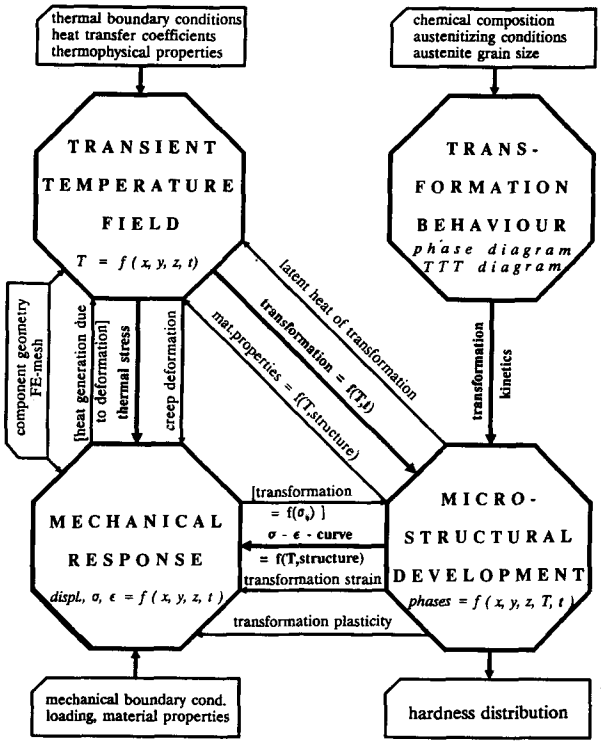

Fig. 1. General system overview to predict the thermomechanical behavior of low alloy steels. Interactions in brackets [ ] are not taken into account.

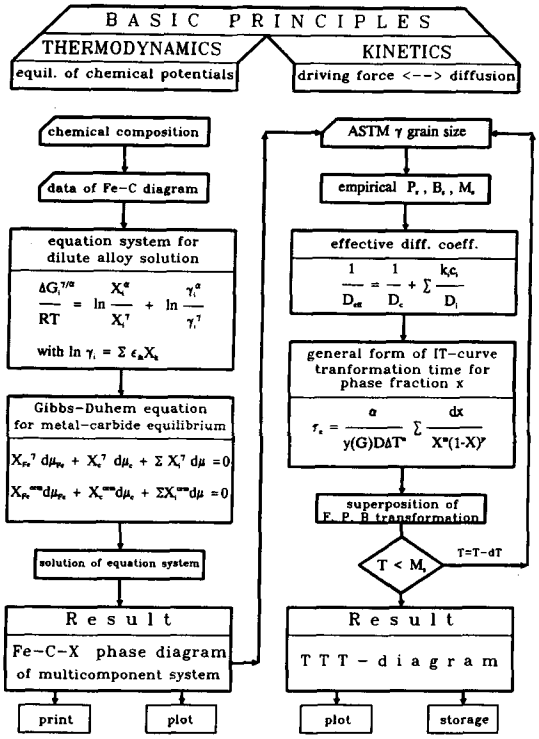

Fig. 2. Flow chart of calculation of the multicomponent phase diagram and the TTT diagram for low alloy steels.

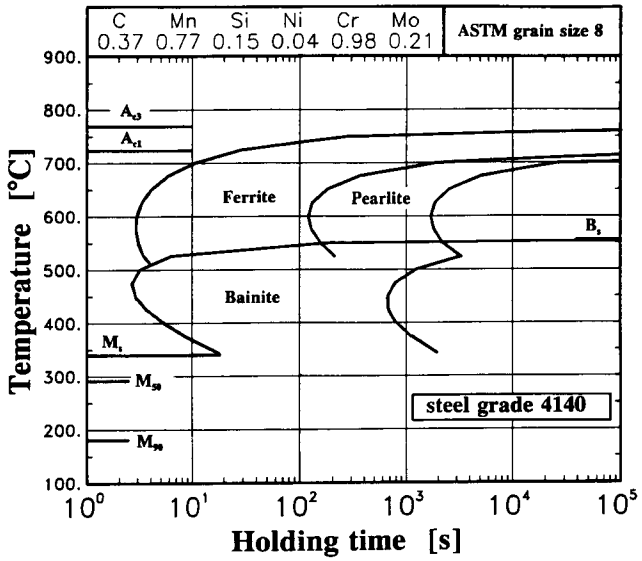

Fig. 3. Calculated TTT diagram for steel grade 4140 assuming an austenite grain size of ASTM 8.

cessing part of the microstructural calculations. A schematic overview of the essential components of the prediction of the phase diagram (Fe–C–X) and time–temperature transformation (TTT) diagram is given in Figure 2. Further details can be found in the aforementioned references, and a later section. In this study the low alloy steel type 4140 was chosen as reference material. For an ASTM grain size 8 the TTT diagram shown in Figure 3 was calculated. The chemical composition and the calculated transformation temperatures are also given in Figure 3. These data on the transformation kinetics of the reference steel, namely 0.1% start- and end-curves of phase transformations as well as the times for intermediate amounts of transformed phases are stored for later use to calculate the transient microstructural changes during cooling.

In application over several years it has been demonstrated that this algorithm gives reliable predictions of the inherent transformation behavior for the full range of hardenability steels.

Coupled Transient Heat Transfer and Microstructural Computations

There is a considerable volume of literature describing finite element modelling for the purpose of computing the transient temperature fields and the mechanical material responses under quenching conditions. Several approaches couple the temperature and microstructural computation in a proper way [9–11] wherein the transfer from isothermal conditions to continuous cooling conditions is carried out using a time–temperature integration of the Avrami equation

$$[X = 1 - \exp(-b \cdot t^n)],$$

b and n being fitted to observations for each individual steel grade as a function of transformation temperature. In our model sufficiently complete TTT diagram data (either predicted as shown in Figure 3 or measured) can be used to calculate the transformation behavior for any cooling condition. In addition, mixed cooling treatments like austempering can be dealt with. The start temperatures for ferrite, pearlite, and bainite are determined for each element. The lowering of the M_s temperature caused by carbon enrichment of austenite during diffusional transformation is also taken into account. A flow chart for this coupled computation is shown in Figure 4. The FE mesh used is illustrated in Figure 5. The partitioning of the elements was chosen so that the volumes of the elements are similar in the radial direction but are smaller at the water quenched end.

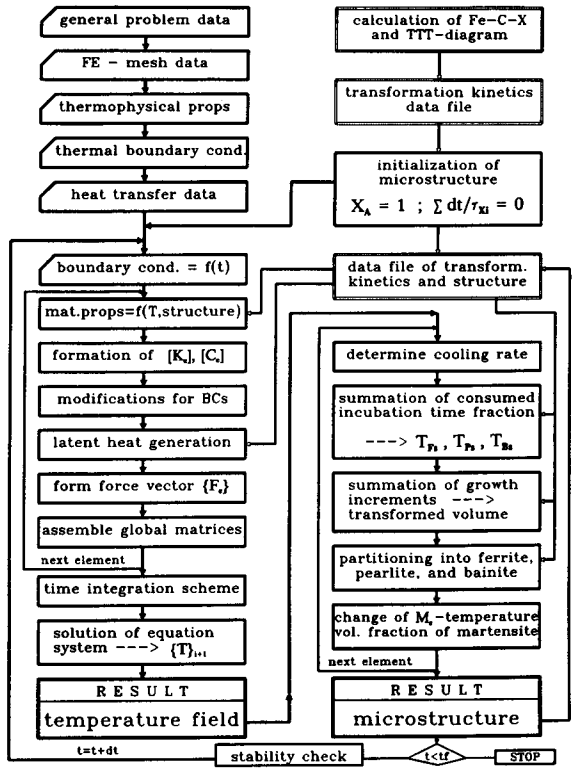

Fig. 4. Flow chart of coupled transient temperature field and microstructural calculation during cooling from the austenite region.

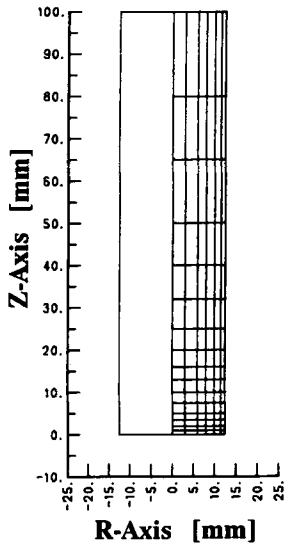

Fig. 5. Used FE mesh of the Jominy specimen for temperature and stress computations.

Mathematical Formulation for the Temperature Field

The differential equation for heat transfer in an axisymmetrical structure can be written in cylindrical coordinates as

$$k_r \frac{\partial^2 T}{\partial r^2} + \frac{k_r}{r}\frac{\partial T}{\partial r} + k_z \frac{\partial^2 T}{\partial z^2} + \dot{Q} = \rho c \frac{\partial T}{\partial t} \tag{1}$$

where k_r and k_z are the thermal conductivities, ρ is the density, c is the specific heat per unit volume, and $\dot{Q}$ is the latent heat release rate during phase transformation, and the boundary condition can be described by

$$k_r \frac{\partial T}{\partial r} l_r + k_z \frac{\partial T}{\partial z} l_z + h(T - T_F) + \sigma\varepsilon(T^4 - T_F^4) = 0 \tag{2}$$

wherein h is the convective heat transfer coefficient, σ is the Stefan-Boltzmann constant, ε is the emissivity, and T_F is the fluid temperature. l_r and l_z are the cylindrical coordinates.

In the finite element formulation [12,13] the spatial discretization of the governing Fourier equation results in a system of simultaneous ordinary differential equations which can be written in matrix form as

$$[C]\{T(t)\} + [K]\{T(t)\} = \{F\} \tag{3}$$

where $[K]$ is the thermal conductivity matrix, $[C]$ is the heat capacitance matrix, and $[F]$ is the thermal force vector.

The discretization in time requires an optimum finite difference algorithm to achieve both numerical stability and rapid convergence. The general form of the difference schemes can be written in the form [12]

$$([C] + \Theta\Delta t[K])\{T\}_{i+1} = ([C] - (1 - \Theta)\Delta t[K]) \cdot \{T\}_i + \Delta t((1 - \Theta)\{F\}_i + \Theta\{F\}_{i+1}) \tag{4}$$

or more generally

$$[A]\{T\}_{i+1} = [P]\{T\}_i + \{F^*\} \tag{5}$$

Depending on the value for Θ, the associated methods are

- $\Theta = 0$—forward difference method
- $\Theta = \frac{1}{2}$—central difference or Crank-Nicholson method
- $\Theta = \frac{2}{3}$—Galerkin's method
- $\Theta = 1$—backward difference method

The solution process for the time dependent field problem is, however, numerically difficult (see [12]). To satisfy physical reality the diagonal coefficients in $[A]$ must be positive and the off-diagonal values should be negative. Numerical oscillations in the values of $\{T\}_{i+1}$ are related to the eigenvalues of the matrix product $[A]^{-1} \cdot \{P\}$. If they are all positive, stable calculation is reached; if some are negative but greater than -1 one gets stable calculations but numerical oscillations; if some are less than -1 then the calculation will be unstable. These findings lead to the necessary condition for control of the time step in the form

$$\Delta t \leq \frac{ks^2}{\lambda(1 - \Theta)}, \tag{6}$$

wherein k is a constant and s is the smallest distance in the mesh. A similar condition can be obtained from consideration of the Fourier number $[F = \rho cs^2/(\lambda\Delta t)]$, which should have a value of approximately unity.

Another improved iterative method is the "residual heat" or "redistribution method" for the solution of nonlinear problems involving variable material properties as suggested in [14]. A comparison of one-step and high order step schemes was made in [15], wherein the Crank-Nicholson scheme exhibited the

best error constant of the one-step methods. Therefore in this work the Crank-Nicholson scheme ($\Theta = \frac{1}{2}$) was used for the numerical integration. The critical step size required to avoid numerical oscillations was 0.25 *s*.

Initial and Boundary Conditions

The FE program allows one to consider various boundary conditions such as

- free or forced convection at the surface with $h = f(T$, phase amount)
- heat flux defined across the boundary
- radiation at the surface
- prescribed or measured temperatures as a function of time
- use of the quenching power H for different cooling media [16,17]

The thermal properties are temperature and microstructure dependent and a linear mixture rule is used, that is, $\lambda = \Sigma \lambda_i \nu_i$, where ν_i is the amount of the phases (A, F, P, B, M; $i = 1, 5$). In addition the latent heat for ferrite, pearlite, bainite, and martensite formation was introduced using the following values: $Q_F = 5.9\ 10^8$, $Q_P = 6.0\ 10^8$, $Q_B = 6.2\ 10^8$ and $Q_M = 6.5\ 10^8$ J/m^3). The rate of the heat source can then be described by the equation $\dot{q} = \Sigma Q_i \partial \nu / \partial t_i$. The heat transfer coefficients used for the water quenching as well as those for radiation and convection for the surfaces exposed to the air are shown in Figure 6.

Calculation of Microstructural Phase Changes

Coupled with the temperature field calculation, the microstructure for each element at every time step

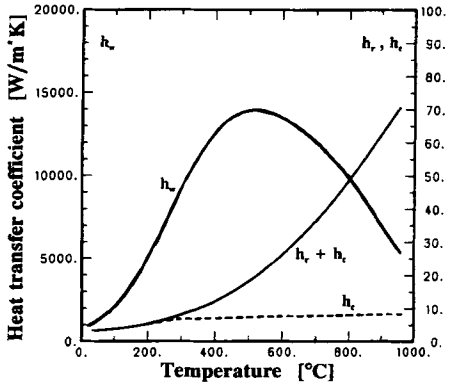

Fig. 6. Heat transfer coefficient for water cooling, free convection and radiation ($\varepsilon = 0.5$) in air.

was calculated. Retrieving the stored TTT data the transformation start temperature (0.1%) is calculated by an integration of the portions of consumed time over the thermal cycle. The temperatures at which particular transformed phase amounts have been formed are calculated from the Avrami Rule

$$\int_{T_i}^{T_f} \frac{dt}{\tau(X_i, T)} = 1 \tag{7}$$

where $\tau(X_i, T)$ is the transformation time for a volume fraction X_i of phase i at temperature T and this can be described analytically in the general form

$$\tau(X_i, T) = \frac{1}{\beta_i^{2(G-1)/2} D_i \Delta T^q} \cdot \int_0^{X_i} \frac{dX}{X_i^{2(1-X_i)/3}(1 - X_i)^{2X_i/3}} \tag{8}$$

where β_i is a kinetic factor [8], G is the ASTM austenite grain size, and D_i is the effective diffusion coefficient. Graphically, this equation gives a typical sigmoidal function between transformed phase amount and time.

Results of Temperature Field and Microstructure Calculation

The surface temperature for different distances from the quenched end of the Jominy sample is shown in Figure 7 as a function of cooling time. The recalescent effect of latent heat liberation on the temper-

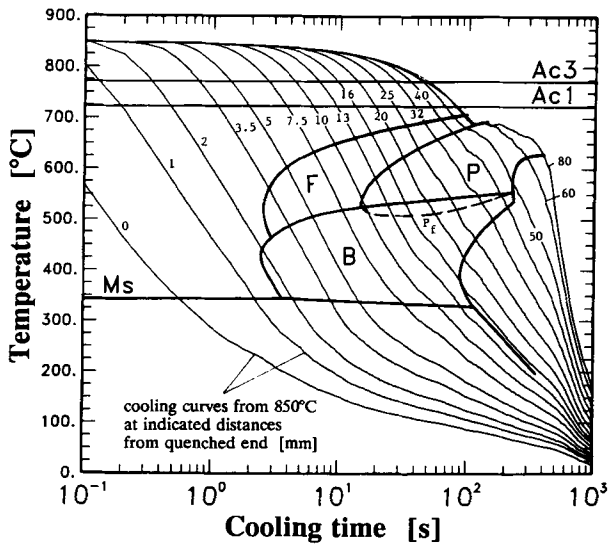

Fig. 7. Plot of temperature profiles for various distances from quenched end including transformation start curves.

ature distribution is especially obvious at low cooling rates. A comparison of the FE results with the curve fitting approach [8] indicates that the analytical formula gives a good estimation for distances from the quenched end between 10 and 30 mm, whereas at larger distances the temperature is clearly underestimated. In addition the calculated start curves for ferrite, pearlite, and bainite formation are drawn in Figure 7.

An isothermal contour plot ot the temperature field after a cooling time of 1 min is given in Figure 8. The effect of radiation at the unquenched end is evident. For reasons of the prediction of hardness and comparisons with conventionally determined CCT diagrams, the cooling rates at 700°C are plotted versus the distance from the quenched end in the upper part of Figure 9, whereas the lower part shows the amount of microstructural constituents after cooling to room temperature. Such distributions are evaluated and stored for each time step and element.

The microstructural evolution at two different distances are shown in Figure 10. The start temperatures for ferrite, pearlite, and bainite formation are plotted in Figure 11 versus the distance from the quenched end.

Finally the hardness distribution can be predicted using the approach described in [18]. The calculated Jominy hardness curve for the steel grade 4140 is plotted in Figure 12. The hardness distribution in the radial direction can also be evaluated.

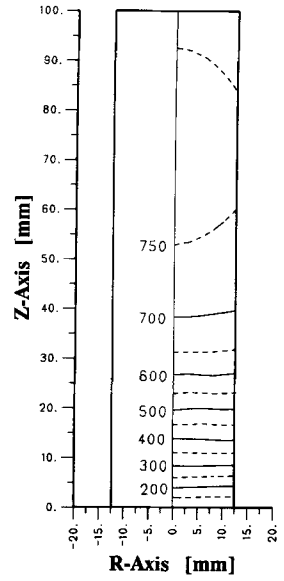

Fig. 8. Contour plot of isotherms in the cross section of the Jominy specimen after a cooling time of 1 min.

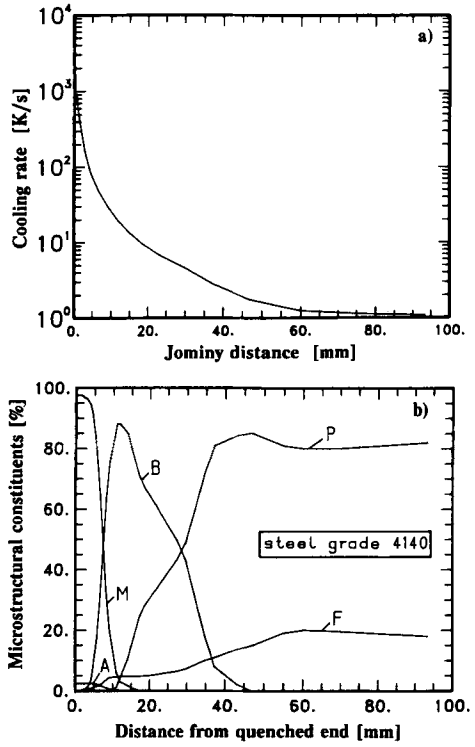

Fig. 9. Amount of microstructural constituents and cooling rate at 700°C vs. distance from the quenched end.

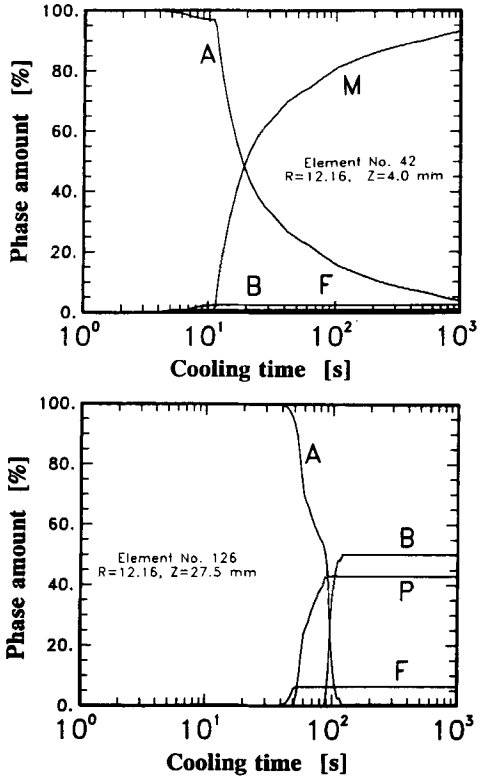

Fig. 10. Microstructural evolution at quenched end of the Jominy specimen and at a distance of 4 mm and 27.5 mm.

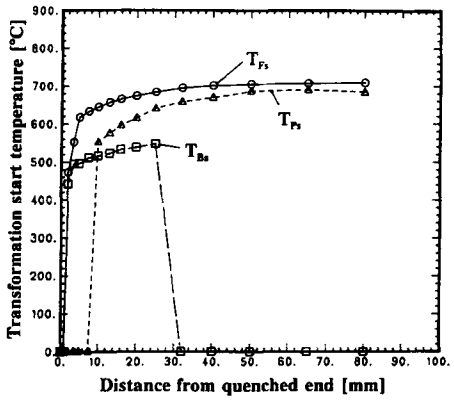

Fig. 11. Calculated ferrite, pearlite and bainite start temperatures vs. the distance from the quenched end.

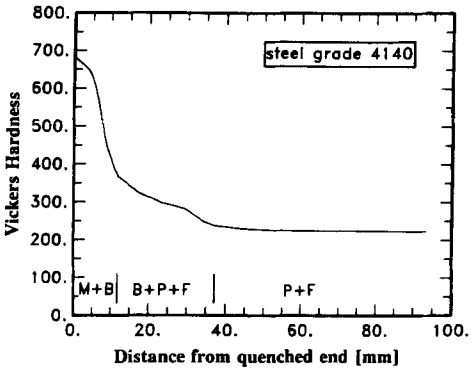

Fig. 12. Calculated hardness profile for the Jominy specimen using the chemical composition data for steel grade 4140 and cooling rates at 700°C.

Computation of the Mechanical Response

Mathematical Formulation of the Stress/Strain Calculation

For the description of the thermoelastic–plastic material behavior the incremental plasticity approach was used in this work. The constitutive equation can be expressed as the sum of the incremental strains

$$\{\partial\varepsilon\} = \{\partial\varepsilon_e\} + \{\partial\varepsilon_{th}\} + \{\partial\varepsilon_p\} + \{\partial\varepsilon_{tr}\} + \{\partial\varepsilon_{tp}\} \quad (9)$$

where $\partial\varepsilon_e$ is the elastic, $\partial\varepsilon_{th}$ the thermal, $\partial\varepsilon_p$ the plastic, $\partial\varepsilon_{tr}$ the transformation, and $\partial\varepsilon_{tp}$ the transformation plasticity strain increment. The strain rate and temperature dependent flow curves were approximated by a polynomial function as used in [13,19]:

$$\sigma = E\varepsilon \Big/ \left\{1 + \left[\frac{E\varepsilon}{(1 - E'/E)\sigma_k + E'\varepsilon}\right]^n\right\}^{1/n} \quad (10)$$

where σ_k is the stress level at the intersection of the elastic and plastic deformation branches and E' is the plastic modulus. In addition, a transformation of the flow curve from the uniaxial to the multiaxial stress state is made. The plastic strain increments are obtained using the classical theory of plasticity with the von Mises yield criterion in association with the Prandtl-Reuss flow relation. Isotropic hardening behavior was assumed for the calculation. Further details are given in [13] where the TEPSAC code is described and this was the starting point for the thermoelastic–plastic stress analysis.

Modifications were made to incorporate the microstructural effects on the mechanical material properties and to describe the dilatation strain and transformation plasticity. The transformation strain was described using the equation

$$\varepsilon_{tr} = \int_{T_a}^{T} \alpha_i \nu_i \, dT \quad (11)$$

with $\alpha_2 = 0.0025$ for ferrite, $\alpha_3 = 0.003$ for pearlite, $\alpha_4 = 0.0045$ for bainite, and $\alpha_5 = 0.008$ for martensite. As described in [10] the transformation plas-

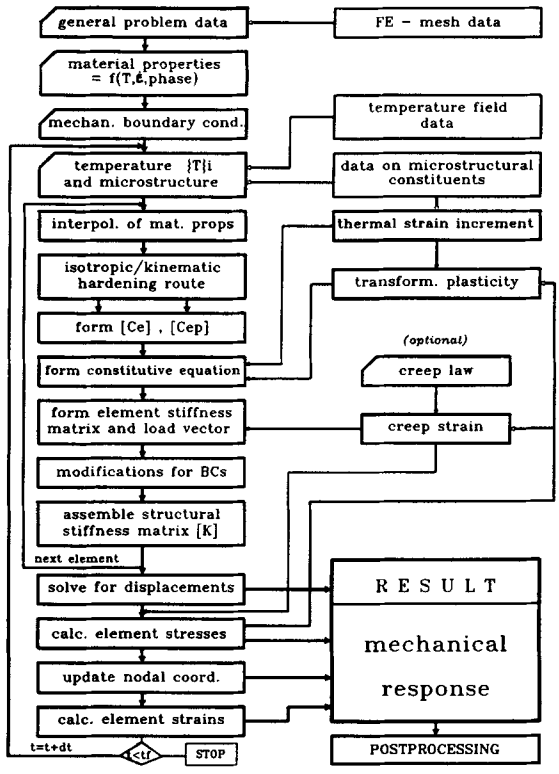

Fig. 13. Flow chart of stress/strain calculation taking into account microstructural effects.

ticity strain increment can be taken to be proportional to the stress deviator in the form

$$\{\partial\varepsilon_{tp}\} = \frac{3}{2} K(1 - X_i)dX_i s_{ij} \qquad (12)$$

A comprehensive explanation of the metallurgical aspects of transformation plasticity and an assessment of the existing approaches are given in [20,21]. A global flow chart of the stress/strain calculation is given in Figure 13.

Results of the Mechanical Stress/Strain Calculations

The calculated dilatation (ε_r vs. time) for an element near the quenched end is shown in Figure 14, which illustrates the volume change during martensite formation. The distortion at the quenched end as a function of cooling time is given in Figure 15 wherein for clarity the displacements are drawn using an expanded scale. As an example for the evaluation of stress components the radial, axial, and hoop stress at the quenched end as a function of time is shown in Figure 16. Starting with a strong trend towards tensile stresses these stress are reversed into compression after formation of martensite. The residual axial stress after complete cooling is shown in Figure 17.

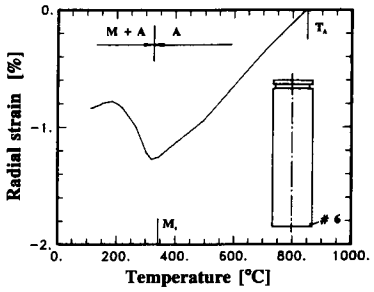

Fig. 14. Thermal and transformation strain for element number 6 (0.5 mm from the quenched end, at the surface).

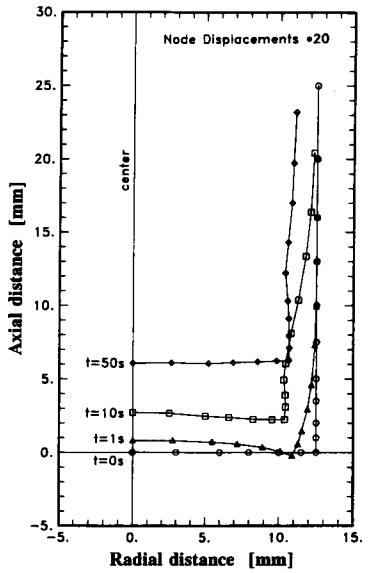

Fig. 15. Distortion at the quenched end during cooling at different cooling times. Note that the node displacements are drawn using a lateral scaling factor of 20.

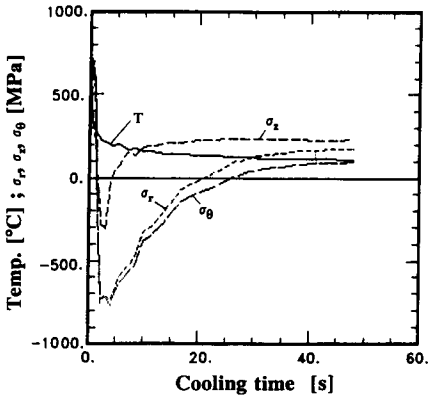

Fig. 16. Stress development near the quenched end [σ_r, σ_t, $\sigma_\Theta = f(t)$].

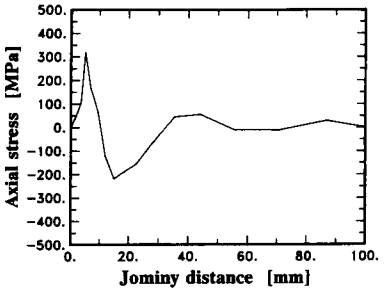

Fig. 17. Residual axial stress after cooling at the surface.

Discussion and Projections for Wider Applicability

The successful predictions of heat transfer, microstructure, and residual stresses in a Jominy specimen illustrates effectively the influence of transformation induced hardenability behavior on the mechanical response of the reference steel 4140. As observed in [22] a linear correlation exists between the hardenability and the residual stresses; that is, the larger the ideal diameter the higher are the maximum axial

stresses. The general scheme, using the coupled, closed loop calculation of the transformation induced hardenability behavior, the temperature distribution, and mechanical stresses enables the reliable prediction of microstructural effects given by the chemical steel composition and heat treatment conditions. Especially in cases where the geometry and the cooling conditions are rather severe, the microstructural effects play a major role. Models of this kind allow the user to identify critical parameters for the onset of serious internal stresses.

As indicated in [10] the influence of the deviatoric stress tensor on the transformation behavior of martensite as well as on diffusional transformations can be important. This effect will soon be implemented within the model, which will then effect a full coupling of all significant interacting effects.

Of great technical importance is the predictability of behavior during and after tempering or stress relief annealing. Anticipating this development the FE program already incorporates a creep strain module which will be applicable to the prediction of relaxation strains and stress reductions. The theoretical and empirical base is already available for predicting the mechanical material properties in the quenched and tempered state; see [23].

Equally significant for future software is that successful applications of the thermodynamic and kinetic transformation part of our model have been developed for predicting the microstructure in weldments [24–26].

In summary, the model and associated modules give more insight and better predictability of the microstructural processes and their influence on the mechanical behavior, thus increasing the potential for optimizing steel structures and heat treatments within increasingly severe design strictures.

All calculations were carried out on the mainframe VAX 8650. The CPU time for the combined FE temperature and stress calculations was about 1 hr. The proposed expansions of the program should be economically accomodated by the next generation of software.

Conclusion

A computer model which simulates the performance of the quenching of an axisymmetric specimen is presented. Based on a thermodynamic and kinetic prediction of the transformation behavior the microstructural evolution during quenching is calculated coupled with the transient temperature field. The model includes the rate of latent heat released by the phase transformations, temperature dependent radiation and convective heat transfer are assumed at the boundary in contact with air or water. The microstructural results are taken fully into account for the prediction of the residual stresses, including phase transformation strain and transformation plasticity. In addition to the mechanical response the hardness distribution is predicted. The calculated results are in good agreement with the experimental findings for the reference material and shape.

Acknowledgments. We would like to acknowledge the assistance of Prof. T.-R. Hsu from the University of Manitoba who lent us his FE software TEPSAC, which was used in part and modified for the extended tasks, of Dr. Sid Feldman of Minitech Ltd. who lent us a part of the package CASIS and Drs. Torsten Ericsson and Bengt Hildenwall of Linköping who introduced us to the literature on transformation induced stresses.

The work was performed during the sabbatical leave of B. Buchmayr at McMaster University under the sponsorship of the Austrian Research Fund in the form of a Schroedinger Stipendium. Additional support was received through a Natural Sciences and Engineering Research Council of Canada grant to J.S. Kirkaldy.

References

1. D.V. Doane and J.S. Kirkaldy (eds.): *Hardenability Concepts with Applications to Steel*, Met. Soc. AIME, Warrendale Pennsylvania, 1978.
2. E. Macherauch and V. Hauk (eds.): *Eigenspannungen. Entstehung-Berechnung-Messung-Bewertung*, Deutsche Gesellschaft fuer Metallkunde, 1983.
3. *Calculation of Internal Stresses in Heat Treatment of Metallic Materials*, Conf at Linköping University, May 1984, in *Material Science and Technology* 1, 1985, Oct. issue, pp. 753–921.
4. E. Macherauch and V. Hauk (eds.): *Residual Stresses in Science and Technology*, Deutsche Gesellschaft fuer Metallkunde, 1987.
5. J.S. Kirkaldy: *Met. Trans.*, 1973, Vol. 4, pp. 2327–2333.
6. J.S. Kirkaldy and E.A. Baganis: *Met. Trans.*, 1978, Vol. 9A, pp. 495–501.
7. J.S. Kirkaldy and R.C. Sharma: *Scripta Metall.*, 1982, Vol. 16, pp. 1193–1198.
8. J.S. Kirkaldy and D. Venugopalan: *Phase Transformation in Ferrous Alloys*, A.R. Marder and J.I. Goldstein, eds., AIME, Philadelphia, 1984, pp. 125–148.
9. B. Hildenwall and T. Ericsson: in [1], p. 579.
10. S. Denis, S.S. Joestroem and A. Simon: *Met. Trans.*, 1987, Vol. 18A, pp. 1203–1212.
11. S. Kamamoto, T. Nishimori and S. Kinoshita: *Mat. Science and Technology*, 1985, Vol. 1, pp. 798–804.

12. L.J. Segerlind: *Applied Finite Element Analysis*, 2nd ed., John Wiley & Sons, New York, 1984.
13. T.-R. Hsu: *The Finite Element Method in Thermomechanics*, Allen & Unwin, Boston, 1986.
14. G. Beer and J.L. Meek: in: Proc. Conf. on Finite Element Methods in Engineering, Univ. of New South Wales, Australia, 1974, V.A. Pulmano and A.P. Kabaila, eds., pp. 729–739.
15. M.A. Hogge: in: *Numerical Methods in Heat Transfer*, R.W. Lewis, K. Morgan and O.C. Zienkiewicz, eds., John Wiley & Sons, 1981, pp. 75–90.
16. C.A. Siebert, D.V. Doane and D.H. Breen: *Hardenability of Steels—Concepts, Metallurgical Influences and Industrial Applications*, ASM, Metals Park, Ohio, 1977.
17. K.-E. Thelning: *Steel and its Heat Treatment*, 2nd ed., Butterworths, London, 1984, p. 147.
18. P. Maynier, B. Jungmann and J. Dollet: in [1], p. 518.
19. R.M. Richard and J.R. Blacklock: *AIAA J.*, 1969, Vol. 7 (3), pp. 432–438.
20. W. Mitter: *Umw and lungsplastizitaet und ihre Beruecksichtigung bei der Berechung von Eigenspannungen*, Metallkundl. Techn. Reihe 7, Gebr. Borntraeger Verlag, Stuttgart, 1987.
21. S. Denis and A.S. Simon: *Residual Stresses in Science and Technology*, E. Macherauch and V. Hauk, eds., DGM-Verlag, 1987, Vol. 2, pp. 565–572.
22. P. Graja, H. Mueller and E. Macherauch: *Eigenspannungen. Entstehung-Messung-Bewertung*, E. Macherauch and V. Hauk, eds. Deutsche Gesellschaft fuer Metallkunde, Vol. 1, 1983, pp. 189–210.
23. D. Venugopalan and J.S. Kirkaldy: in [1], pp. 249–267.
24. B. Buchmayr and H. Cerjak: Proc. IIW Int. Conf. on *Improved Weldment Quality with Special Reference to Computer Technology*, Vienna, 1988, Pergamon Press, pp. 43–50.
25. D.F. Watt, L. Coon, M. Bibby, J. Goldak and C. Henwood: *Acta Metall.*, 1988, Vol. 36 (11), pp. 3029–35.
26. C. Henwood, M. Bibby, J. Goldak and D. Watt: *Acta Metall.*, 1988, Vol. 36 (11), pp. 3037–46.

Received March 17, 1990.